P7.9 OPERATIONAL EVALUATION OF THE REAL-TIME ATTENUATION CORRECTION SYSTEM FOR CASA IP1 TESTBED

Y.X. Liu, Y.T. Wang, D. Willie, V. Chandrasekar and V.N. Bringi
Colorado State University, Fort Collins, Colorado

1. INTRODUCTION

Collaborative Adaptive Sensing of the Atmosphere (CASA) Engineering Research Center pursues a network centric paradigm to sample the atmosphere with small, low cost X-band radars as opposed to traditional long range S-band radars (McLaughlin et al. 2005). The first generation testbed of CASA, called Integrated Project 1 (IP1), is currently operational in Oklahoma, US. This provides us a platform to validate, verify, and expand the network centric paradigm. In doing so, many efforts have been contributed to validate and improve solutions for the associated engineering challenges of using X-band radar systems (Chandrasekar et al. 2004). In this paper, we evaluate particularly the real-time attenuation correction system for CASA IP1 testbed using data collected during the past year, with emphasis on those collected during the recent field experiment (since Apr 2007).

2. ATTENUATION CORRECTION

2.1 Background

In rain, radar attenuation is due to scatter and absorption of eletromagnetic waves by the rain drops. It is well known that the attenuation due to rain is a function of multiple independent variables such as water content, temperature, and frequencies (Bringi and Chandrasekar 2001). At X-band frequencies the attenuation is significant and cannot be neglected. Because it is a cumulative effect over the radar propagation path, the attenuation causes negative bias in the radar reflectivity. Moreover in dual-polarization radar systems (e.g., CASA IP1), it attenuates both reflectivity at horizontal-polarization (Z_h) and vertical-polarization (Z_v), and consequentially the differential reflectivity (Z_{dr}) between the two polarizations because the shape of rain drops is oblate. If Z_h and Z_{dr} are used to derive rainfall rate, to classify hydrometeor particle types, or to study rain microphysics, the attenuation should be considered and corrected. Viewing attenuation correction data is important to the end user community. Therefore attenuation correction has been a continuous effort since the inception.

There are several available techniques (e.g., Hitschfeld and Bordan 1954, Bringi et al. 1990, Testud et al. 2000, Bringi et al. 2001) to correct Z_h and Z_{dr} for rain-induced attenuation. Hitschfeld and Bordan (1954) derived an equation to correct reflectivity for attenuation in terms of only the measured reflectivity. It is known that this method is unstable and it is not recommended to correct for attenuation. Nonetheless, the HB method has become a basic building block for many attenuation algorithms with an additional constraint typically acquired by independent measurement of the total path integrated attenuation (PIA). If dual-polarization and differential propagation phase (Φ_{dp}) are available, it has been shown that the rain attenuation can be fairly well estimated. Bringi et al. (1990) showed that specific attenuation at h-polarization (A_h in dB/km) can be related to specific differential propagation phase (K_{dp} in deg/km) almost linearly in the form $A_h = \alpha K_{dp}$ for frequencies below about 20 GHz. Therefore the attenuation can be directly estimated from the measured Φ_{dp} since Φ_{dp} is the range integral of K_{dp}. Testud et al. (2000) gave a solution for A_h using a technique (termed the ZPHI algorithm) with Φ_{dp} constraint similar to the rain profiling techniques originally developed for space-borne radars. Both methods above can render a stable estimation of A_h. However, the coefficient (α) in the A-K_{dp} relationship is fixed *a priori* and therefore the attenuation estimation is only as good as the *a priori* coefficient itself. Since α can vary over a wide range (e.g. 0.075-0.65 dB/deg at X-band) due to change in temperature, drop shape models (Thurai et al. 2007) and the raindrop size distributions (DSD) to a lesser degree, it is important to estimate α, especially at X-band. Bringi et al. (2001) gave a method to estimate α for C-band radars by invoking self-consistency with the measured Φ_{dp}. Park et al. (2005a,b) adapted the self-consistent method for X-band radars. In summary extensive background research has been conducted to get ready for implementing attenuation correction.

2.2 Real-time Attenuation Correction System for CASA IP1

It is worth noting that CASA is a real-time system. The user-polling data model is at the heart of such real-time system (McLaughlin et al. 2005). This gives rise to challenges of distributing system resources wisely in order to render real-time response within a system 'heart-beat', which defines the average response time of the system. Within a 'heart-beat', the system could be performing routine scanning or be rapidly re-positioned to scan where it attracts most interests and attentions in case of a severe weather event. Certainly this can pose more constraints on algorithms design and implementation. With this guideline, the attenuation correction system for CASA is tailored to balance well with the rest of system components to share the resources.

Liu et al. (2006a) described an improved rain attenuation correction algorithm for reflectivity and differential reflectivity, which extend the self-consistent method in certain important technical and practical

**Corresponding author address*: Yuxiang Liu, Colorado State Univ., Dept. of Electrical and Computer Engineering, Fort Collins, CO 80523; e-mail: liuyx@engr.colostate.edu.

aspects. This is the attenuation correction algorithm running in the CASA IP1 system (here after the IP1 ACA). A brief summary is given as follows.

Considering attenuation, the 'intrinsic' reflectivity (Z^e) in mm^6m^{-3} and the measured reflectivity (Z^m) in mm^6m^{-3} at range *r* is expressed as,

$$Z^e(r) = Z^m(r)\exp\{0.46\int_{r_0}^{r} A(s)ds\}. \tag{1}$$

where r_0 is the beginning range of a raincell where attenuation is being considered, *r* is the current range gate, and $A(r)$ is the specific attenuation profile (in dB/km).

Eq. 1 is the basic equation to correct measured reflectivity for attenuation. The $A(r)$ profile is the unknown to be solved here. Testud et al (2000) gave a solution for A_h(r) in rain with Φ_{dp} constraint as,

$$A_h(r) = \frac{[Z_h^m(r)]^b[\exp\{0.23\alpha b\Delta\Phi_{dp}(r_0,r_i)\}-1]}{I(r_0,r_i)+[\exp\{0.23\alpha b\Delta\Phi_{dp}(r_0,r_i)\}-1]I(r,r_i)}. \tag{2}$$

where the subscript *h* denotes horizontal polarization, $\Delta\Phi_{dp}(r_0,r_i)$ is the difference of $\Phi_{dp}(r_i)$ - $\Phi_{dp}(r_0)$, *b* is the exponent of the HB attenuation-reflectivity model, and $I(r_1,r_2)$ is a quantity defined as,

$$I(r_1,r_2) = \int_{r_1}^{r_2} 0.46b[Z_h^m(s)]^b ds. \tag{3}$$

The IP1 ACA for reflectivity follows the self-consistency principle (Bringi et al. 2001) however with following modification for attenuation correction,

$$\Phi_{dp}^m(r) = \Phi_{dp}^c(r,\alpha) + e(r). \tag{4}$$

where the superscript *m* denotes the measured quantity, the superscript *c* denotes the modeled quantity which is defined in next equation (eq. 5), and $e(r)$ is the modeling error which is assumed to be normal.

$$\Phi_{dp}^c(r,\alpha) = 2\int_{r_0}^{r}\frac{A(s,\alpha)}{\alpha}ds; r_0 \le r \le r_i. \tag{5}$$

It is now clear that $e(r)$ is a non-linear cost function to be minimized with respect to α (see eqs. 4, 5 and 2). The IP1 ACA minimizes this cost function in a least squares sense. It is implemented very efficiently so that it is computationally efficient compared to the original method. It is demonstrated that the final α (if it can be found) with acceptable precision rarely needs more than 5 iterations to converge (Liu et al. 2006a).

While the attenuation correction for Z_h follows closely the self-consistent principle, the IP1 ACA for correcting Z_{dr} is completely different than that in Bringi et al. 2001. Given the advantage of fast least squares search method, the attenuation correction for Z_{dr} can start with correcting the Z_v first using the same principle. This is based on the assumption that A_v is approximately linear to K_{dp}, which is reasonably valid under rain condition. The minimization of $e(r)$ in eq. 4 (but now with Z_m^v as input) will retrieve an α_v which is used to correct Z_v. The corrected Z_{dr} can be simply retrieved by,

$$Z_{dr}^e(r) = \frac{Z_h^e(r)}{Z_v^e(r)}. \tag{6}$$

It is worth noting that this Z_{dr} method has a practical value that the retrieved differential attenuation (A_{dp}) is immune to the Z_{dr} system bias. In other words, the Z_{dr} system bias has no range distortion effects on the estimated A_{dp} and can be adjusted either prior to or after the attenuation correction.

3. DATA COLLECTION AND PREPROCESSING

3.1 Data Flow

IP1 consists of four identically designed X-band dual-polarization Doppler radars located in Chickasha (KSAO), Cyril (KCYR), Lawton (KLWE), and Rush Springs (KRSP), respectively. Software running at the node-level includes time series daemon, spectrum processing for velocity, clutter suppression, attenuation correction, etc. The processed data are then compressed and sent to the central server, namely SOCC located in the National Severe Storm Laboratory (NSSL) in Norman, Oklahoma (Brotzge et al. 2005). Fig.1 gives an overview of the current topology of IP1.

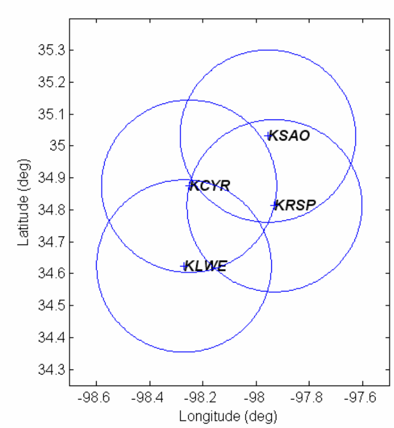

Figure 1. Toplogy of the four X-band dual-polorization Doppler radar nodes in CASA IP1 testbed. In counter-clockwise order: KSAO (in Chickasha), KCYR (in Cyril), KLWE (in Lawton), and KRSP (in Rush Springs). Circles are 30 Km range rings.

3.2 Preprocessing For Attenuation Correction

At the heart of the IP1 ACA is the non-linear least squares method for estimation of α_h and α_v. But in many situations, one often finds the raw data need preprocessing for data quality control. For the IP1 ACA the quality of measured Φ_{dp} is particularly important. Therefore, prior to the IP1 ACA, the measured Φ_{dp} is run through a series of tests to assure it is suitable for the use of rain attenuation correction purpose as follows,

1. Is the system Φ_{dp} set to a proper value such that unfolding is not necessary or at least minimum?
2. Is there one rain cell or more encountered in the propagation path?
3. Is the increment ($\Delta\Phi_{dp}$) sufficiently large to carry out the numerical process?

Test 1 is particularly important to avoid situation when Φ_{dp} falls into discontinuity region of the estimating function (e.g., -180 deg and +180 deg). Although the initial system Φ_{dp} of the transmitted pulses can be estimated quite accurately by looping the transmitted pulses through an attenuator back into the receiver, the initial Φ_{dp} of the received signals is difficult to know at the processing level. The total system Φ_{dp} is the sum of both. For the purpose of attenuation correction, a practical solution to this problem is to find a region where stable Φ_{dp} exists over some distance (within which rain is encountered presumably) and reset the system Φ_{dp} to some value where the folding of Φ_{dp} is unlikely to happen. Fig. 2 shows a raw measured Φ_{dp} and the adjusted Φ_{dp} using the above method.

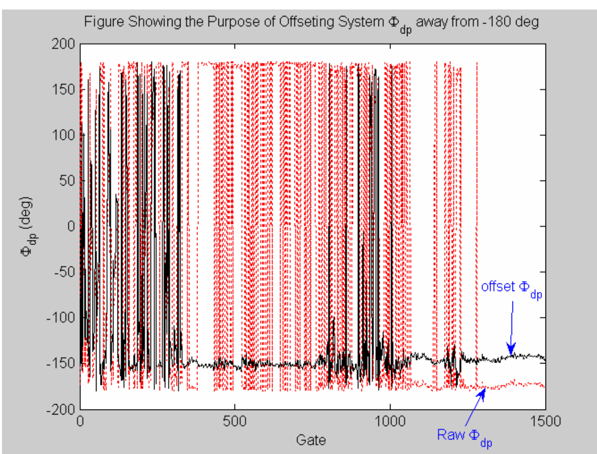

Figure 2. An example of resetting the total system Φ_{dp}. The red dotted line is the measured Φ_{dp} profile. Before resetting, the system Φ_{dp} is very close to -180 degs. Because of this, even very small measurement noise will cause Φ_{dp} values to flip between -180 degs and +180 degs. The black solid line is the offset measured Φ_{dp} profile where the system Φ_{dp} is offset to around -150 degs to avoid the discontinuity.

Test 2 is to identify where to begin and where to stop the rain attenuation correction based on the Φ_{dp} profile. It is known that the variance of Φ_{dp} is different when it is in rain, in mixed phase, in clutter, and has no echo. A simple hard-decision bound logic is built in the IP1 ACA to distinguish each of these sections base on the variance of Φ_{dp}, the co-polar correlation coefficient (ρ_{hv}), and the signal-to-noise ratio (*SNR*). This is to assure that the attenuation correction is carried in a rain region (other than mixed phase, clutter, clear air and etc) because the rain attenuation correction model is not valid otherwise. For the mixed phase attenuation correction it should be treated differently (Liu et al. 2006b).

Test 3 is to ensure the $\Delta\Phi_{dp}$ is sufficiently large to allow α_h and α_v to be estimated without worrying the effect of modeling error. This ensures the $\Delta\Phi_{dp}$ is large enough to generate sufficient range of K_{dp} values which span the drop-shape model curves. Otherwise the self-consistent estimation for α_h and α_v is turned off and a simple attenuation correction method using A_h-K_{dp} and A_{dp}-K_{dp} relationships with *a priori* coefficients is used. In summary an elaborate data handling scheme is used to ensure the IP1 ACA works in real time automatically.

4. EVALUATION

4.1 Self-consistency Check

A squall line event on May 8 2006 is analyzed here. The storm was moving from northwest to southeast and strong attenuation was observed. Fig. 3 shows the 2D histogram (in log scale) of Z_{dr} vs. Z_h before and after attenuation correction. In rain the Z_{dr} is positive and can be approximately linearly related to Z_h. Fig. 3b shows this trend after the attenuation correction, which agrees with theoretical results (Chandrasekar et al. 2004).

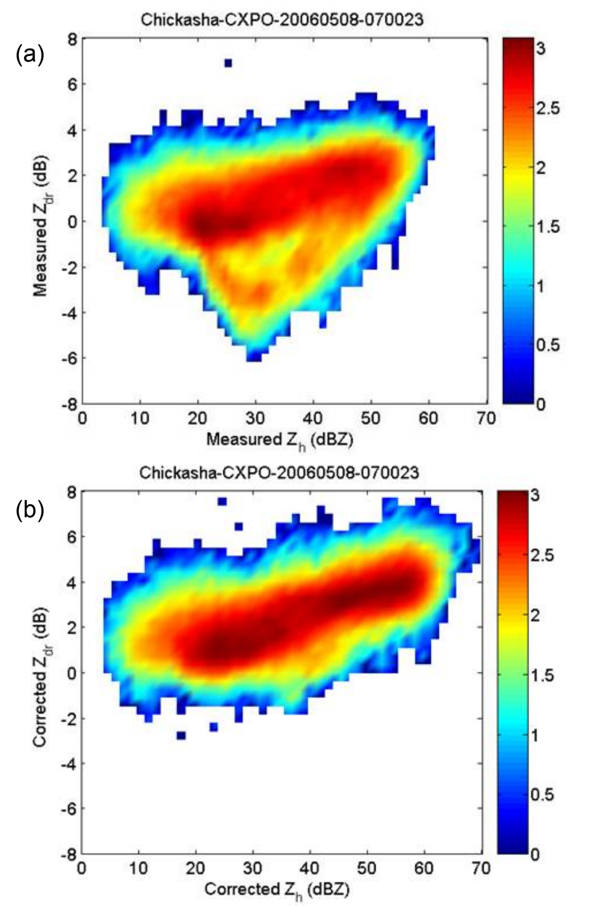

Figure 3. Z_{dr} vs. Z_h 2D histogram (in log scale) of a squall line event at 07:00:23 May 8 2006 UTC. (a) Z_{dr} vs. Z_h before attenuation correction. (b) Z_{dr} vs. Z_h after attenuation correction.

Fig. 4 shows a similar 2D histogram but for K_{dp} vs. Z_h before and after attenuation. It shows that after attenuation correction, the K_{dp} vs. Z_h agrees with theoretically expected range for X band (Chandrasekar et al. 2004).

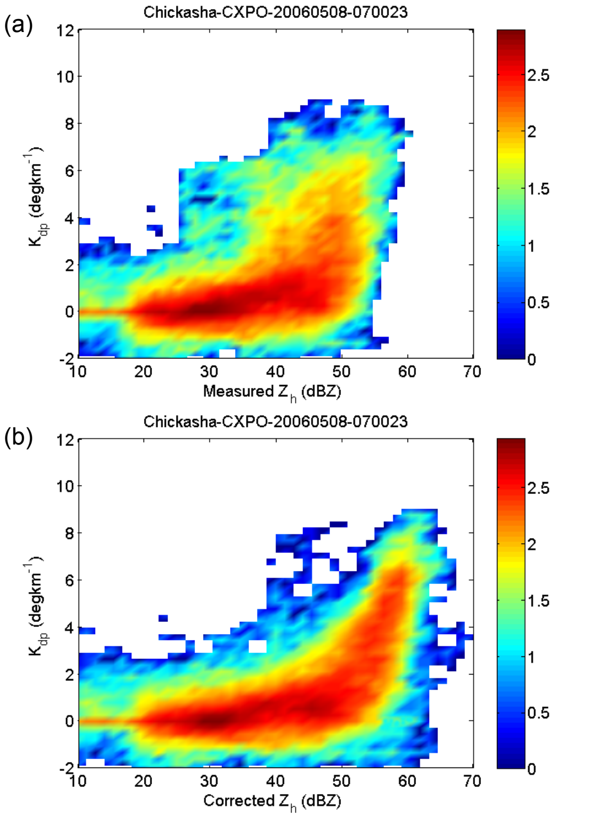

Figure 4. K_{dp} vs. Z_h 2D histogram of a squall line event at 07:00:23 May 8 2006 UTC. (a) K_{dp} vs. Z_h before attenuation correction. (b) K_{dp} vs. Z_h after attenuation correction.

4.2 CASA IP1 and Nexrad Comparison

There is Nexrad coverage over the CASA IP1 testbed, with the closest two WSR-88D (S-band) radars, namely, KFDR and KTLX, at some 100 Km distance from the center of the IP1 network. The resolution, frequencies, and look angles of the CASA IP1 and Nexrad are different. Moreover, although the projections to the earth surface of two range bins from the two systems can be in the same location, their heights can be quite different (e.g. CASA IP1 at about 500m height from a 2 deg elevation beam at 15 Km range, Nexrad at about 1500m height from a 0.5 deg elevation beam at 100 Km range). Nonetheless, the comparison can still provide some insight into how the attenuation correction performs when compared against a non-attenuating radar system.

Fig. 5 shows a storm over the center of IP1 testbed at around 07:37:31 May 8 2007 UTC. Fig. 5a shows the composite reflectivity from the four IP1 radars before attenuation correction. Fig. 5b shows the composite reflectivity after attenuation correction. Fig. 5b is to be compared against visually Fig. 5c which shows the Nexrad reflectivity at almost the same time from the KTLX radar from some 100 Km away. As Fig. 5b and Fig. 5c show, the two reflectivity maps show very similar storm structure although they are from two completely different systems. The improved resolution of CASA data is also to be noted here.

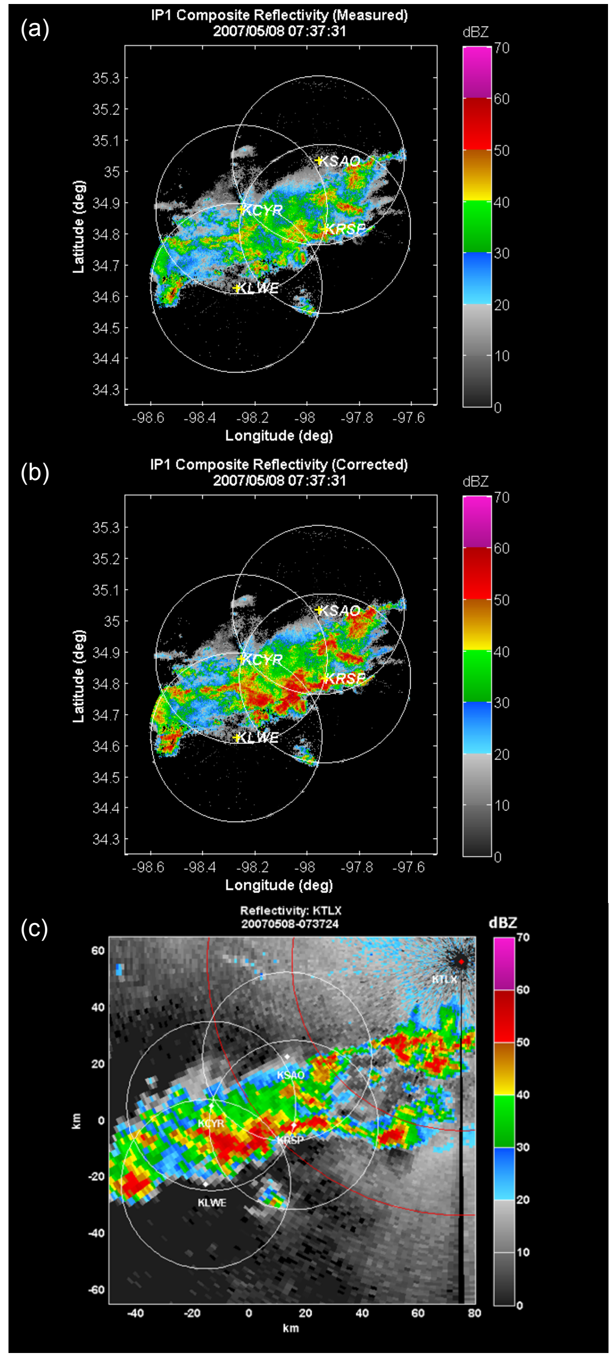

Figure 5. IP1 Reflectivity maps at 07:37:31 May 8 2007 and Nexrad reflectivity map at 07:37:24 May 8 2007. (a) IP1 reflectivity before attenuation correction (b) IP1 reflectivity after attenuation correction (c) Nexrad reflectivity.

4.3 Attenuation Statistics

During the operational phase of CASA IP1 testbed, we observed the beginning of an active spring storm season in Oklahoma. From Apr 10 2007 to May 10 2007, there were at least eight significant storms passed through CASA IP1 testbed. The types of the storms varied from heavy convective to strong squall line. Here we summary the attenuation statistics for days of Apr 10, Apr 11, Apr 24, Apr 27, May 7, May 8, May 9 and May 10. Fig. 6 shows the cumulative distribution function for path integrated attenuation (PIA) obtained from the IP1 ACA. Each statistic used to plot the figure represents the PIA for a radar beam from the beginning of the beam to the end of the beam. The actual length of rain cell within a beam can vary from beam to beam.

Fig. 6 shows that about 80% of the time the PIA is less than 10.79 dB and 90% of the time the PIA is less than 16.93 dB. However, there is situation that the signal is totally extinct after some range when it propagates through a very intensive storm. The statistics of such situation are not represented in this figure. When this happens, part of the storm is missed by one of the radars in the network. The other radars could observe the same part of the storm if the storm is within the overlapping region and the paths are less intensive (see Fig. 1), which is a core component of the CASA concept.

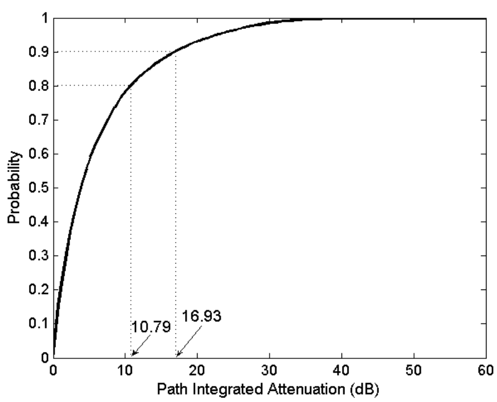

Figure 6. Cumulative distribution function of path integrated attenuation for the storm cases observed in Apr 10, Apr 11, Apr 24, Apr 27, May 7, May 8, May 9 and May 10. All dates are in 2007.

5. CONCLUSIONS

The real-time attenuation correction system for CASA IP1 testbed is evaluated using data collected in the past year. Through the consistency check by using redundancy information in the dual-polarization observables (e.g., Z_{dr}-Z_h, K_{dp}-Z_h relationships), it shows that the IP1 ACA computes the corrected Z_h and the corrected Z_{dr} (after attenuation) within expectation. By comparing with the adjacent Nexrad radar (KTLX) measurement in close space and time, we show that the storm structure is recovered by the reflectivity after attenuation correction and is very similar to that observed by the Nexrad, which operates at non-attenuating frequencies (S-band). We also present about a month of attenuation statistics from the spring experiment, 2007.

6. ACKNOWLEDGEMENT

This work is supported by the Engineering Research Center program of the National Science Foundation (NSF) under the award number 0313747.

References

Bringi, V.N., V. Chandrasekar, N. Balakrishnan, and D.S. Zrnić, 1990: An examination of propagation effects in rainfall on radar measurements at microwave frequencies. J. Atmos. Oceanic Technol., **7**, 829-840.

——, T. D. Keenan, and V. Chandrasekar, 2001: Correcting C-band radar reflectivity and differential reflectivity data for rain attenuation: a self-consistent method with constraints. IEEE Trans. Geosci. Remote Sensing, **27**, 1906-1915.

—— and V. Chandrasekar, 2001: Polarimetric doppler weather radar, principles and applications. Cambridge.

Brotzge, J., D. Westbrook, K. Brewster, K. Hondl, and M. Zink, 2005: The meteorological command and control structure of a dynamic, collaborative, automated radar network. Preprints 21st International Conf. on Interactive Information Processing Systems for Meteor., Ocean., and Hydrology, AMS conf. San Diego, CA.

Chandrasekar, V., S. Lim, N. Bharadwaj, W. Li, D. McLaughlin, V.N. Bringi, and E. Gorgucci, 2004: Principles of networked weather radar operation at attenuating frequencies. Preprints 3rd European Conference on Radar in Meteorology and Hydrology, Visby, Sweden.

Hitschfeld, W. and J. Bordan, 1954: Errors inherent in the radar measurement of rainfall at attenuating wavelengths. J. Meteor., **11**, 58-67.

Liu, Y.X., V.N. Bringi and M. Maki, 2006a: Improved rain attenuation correction algorithm for radar reflectivity and differential reflectivity with adaptation to drop shape models. Preprints IEEE International Geoscience and Remote Sensing Symposium 2006, Denver, Colorado.

——, G.J. Huang, V.N. Bringi and S. van den Heever, 2006b: Estimation of X-band radar attenuation due to wet hail: A simulation study using RAMS supercell case and dual-wavelength (S/X-band) radar. *ERAD06*, 49-52.

McLaughlin, D., V. Chandrasekar, K. Droegemeier, S. Frasier, J. Kurose, F. Junyent, B. Philips, S. Cruz-Pol, and J. Colom, 2005: Distributed collaborative adaptive sensing (DCAS) for improved detection, understanding, and prediction of atmosphere hazards. Preprints 9th Symposium on Integrated Observing and Assimilation Systems for the Atmosphere, Oceans, and Land surface, San Diego, CA.

Park, S.-G., V. N. Bringi, V. Chandrasekar, M. Maki and K. Iwanami, 2005a: Correction of radar reflectivity and differential reflectivity for rain attenuation at X band Part I: theoretical and empirical basis. J Atmos. and Ocean. Technol., **22**, 1621–1632.

——, M. Maki, K. Iwanami, V.N. Bringi and V. Chandrasekar, 2005b: Correction of radar reflectivity and differential reflectivity for rain attenuation at X band Part II: evaluation and application. J Atmos. and Ocean. Technol., **22**, 1633–1655.

Testud, J., E. Le Bouar, E. Obligis, and M. Ali-Mehenni, 2000: The rain profiling algorithm applied to polarimetric weather radar. J. Atmos. Ocean. Technol., **17**, 332-356.

Thurai, M., G.J. Huang, V.N. Bringi, W. L. Randeu and M. Schönhuber, 2007: Drop Shapes, Model Comparisons, and Calculations of Polarimetric Radar Parameters in Rain, J. Atmos. Ocean. Tech., **24**, 1019-1032.